doi:10.1016/j.jmb.2008.01.075 J. Mol. Biol. (2008) 378, 737–748

JMB

Available online at www.sciencedirect.com

ScienceDirect

ELSEVIER

Dynamics of Cholesterol Exchange in the Oxysterol Binding Protein Family

Bertram J. Canagarajah[1], Gerhard Hummer[2]*, William A. Prinz[3] and James H. Hurley[1]*

[1]*Laboratory of Molecular Biology, National Institute of Diabetes and Digestive and Kidney Diseases, National Institutes of Health, U.S. Department of Health and Human Services, Bethesda, MD 20892, USA*

[2]*Laboratory of Chemical Physics, National Institute of Diabetes and Digestive and Kidney Diseases, National Institutes of Health, U.S. Department of Health and Human Services, Bethesda, MD 20892, USA*

[3]*Laboratory of Cell Biochemistry and Biology, National Institute of Diabetes and Digestive and Kidney Diseases, National Institutes of Health, U.S. Department of Health and Human Services, Bethesda, MD 20892, USA*

Received 5 October 2007; received in revised form 4 December 2007; accepted 23 January 2008
Available online 4 February 2008

Edited by M. Levitt

The oxysterol-binding protein-related protein (ORP) family is essential to sterol transfer and sterol-dependent signal transduction in eukaryotes. The crystal structure of one ORP family member, yeast Osh4, is known in apo and sterol-bound states. In the bound state, a 29 residue N-terminal lid region covers the opening of the cholesterol-binding tunnel, preventing cholesterol exchange. Equilibrium and steered molecular dynamics (MD) simulations of Osh4 were carried out to characterize the mechanism of cholesterol exchange. While most of the structural core was stable during the simulations, the lid was partly opened in the apo equilibrium MD simulation. Helix α7, which undergoes the largest conformational change in the crystallized bound and apo states, is conformationally coupled to the opening of the lid. The movement of α7 helps create a docking site for donor or acceptor membranes in the open state. In the steered MD simulations of cholesterol dissociation, we observed complete opening of the lid covering the cholesterol-binding tunnel. Cholesterol was found to exit the binding pocket in a step-wise process involving (i) the breaking of water-mediated hydrogen bonds and van der Waals contacts within the binding pocket, (ii) opening of the lid covering the binding pocket, and (iii) breakage of transient cholesterol contacts with the rim of the pocket and hydrophobic residues on the interior face of the lid.

Published by Elsevier Ltd.

Keywords: cholesterol transfer protein; lipid transfer protein; molecular dynamics simulation; protein conformational change

Introduction

Cholesterol is an important component of mammalian cell membranes and its concentration is tightly regulated.[1–3] The proper distribution of cholesterol and other lipids among intracellular compartments is critical for numerous cellular functions, including signal transduction and membrane trafficking. How this distribution is maintained is poorly understood, but there are two different

**Corresponding authors.* E-mail addresses: hummer@helix.nih.gov; hurley@helix.nih.gov.

Abbreviations used: LTP, lipid transfer protein; OSBP, oxysterol-binding protein; ORP, OSBP-related protein; ORD, OSBP-related domain; MD, molecular dynamics; NPT, constant temperature and pressure; RMSD, root-mean-square deviation.

0022-2836/$ - see front matter. Published by Elsevier Ltd.

modes of lipid transport within cells.[4–6] One is the transfer of lipids through vesicular transport. The other is by a set of specialized proteins called lipid transfer proteins (LTPs), which bind lipids and transfer them between membranes. The oxysterol-binding protein (OSBP)-related proteins (ORPs) are a large family of LTPs conserved from yeast to humans.[7]

The founding member of the ORP family, OSBP, was identified initially because of its ability to bind oxysterols that regulate cholesterol metabolism in mammals.[8] A large number of OSBP homologs were subsequently identified. All contain an OSBP-related domain (ORD) that binds lipids and many have additional domains that may be important for targeting and regulation.[9] Many ORPs bind cholesterol and other sterols as well as oxysterols.[10,11] The strongest evidence that ORPs function as LTPs comes from the yeast *Saccharomyces cerevisiae*, which has seven ORPs (Osh1-Osh7). All of the Osh proteins tested to date are able to transfer cholesterol and others sterols between membranes *in vitro* (W. P., unpublished results).[12] They probably transfer sterols in cells as well; there is a dramatic decrease in the rate of non-vesicular sterol transfer between the endoplasmic reticulum and plasma membrane in a mutant missing all the Osh proteins.[12,13] This mutant also has severe defects in maintaining the proper intracellular distribution of sterols and other lipids, consistent with a role for Osh proteins in lipid transport.[14,15] In addition to functioning as LTPs, Osh proteins and other ORPs have been suggested to have other roles in regulating lipid metabolism and vesicular transport.[7] Some could function as lipid sensors. In mammals, OSBP may regulate other proteins, including phosphatases and the LTP CERT, in response to binding cholesterol.[16,17]

The structures of Osh4 in complex with cholesterol, ergosterol, and various oxysterols have been solved by X-ray crystallography between 1.6 Å and 1.9 Å resolution.[11] The core of the structure is a nearly complete β barrel composed of an antiparallel β-sheet of 19 strands (Fig. 1(a)). Cholesterol binds in the deep hydrophobic tunnel at the center of the β barrel. The top of the tunnel is completely covered by the N-terminal 29 residues of the protein, which is referred to as the lid. The 3-hydroxyl group of cholesterol is buried in the bottom of the pocket, while the alkyl tail interacts with the inner hydrophobic surface of the lid. The closed conformation is stabilized by the interaction of sterol ligands with residues Trp10, Phe13, Leu24 and Leu27 of the lid

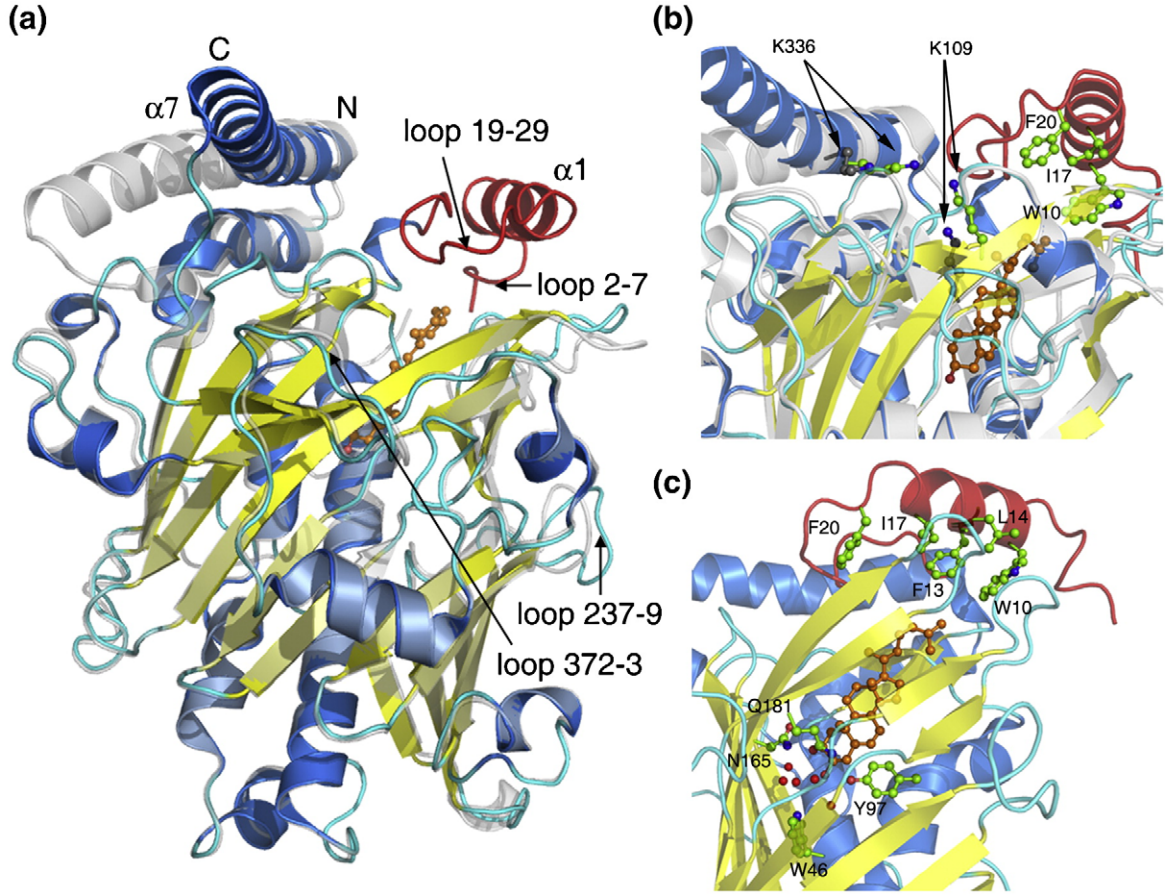

Fig. 1. Overall structure and key features of Osh4. (a) The overall structures of the Osh4-cholesterol complex (red lid, residues 2-29; blue helix and yellow strands, residues 30-434), and the ligand-free truncated Osh4 (grey, residues 30-344). (b) The position of Lys109 and Lys336. (c) Hydration of the cholesterol-binding pocket (water shown as red spheres).

Fig. 1(c). The open side of the β barrel and the bottom of the cholesterol-binding tunnel are closed off by a bundle of helices. The sterol ligands are completely inaccessible to bulk solvent. Cholesterol exchange is thus thought to require opening of the protein.

Several lines of evidence suggest that cholesterol exchange is facilitated by a conformational change in which the lid is displaced from the tunnel and becomes disordered.[11] Some of the highest *B*-factors of the protein are found in the lid region, indicating high mobility. The lid is also one of the regions of the protein most susceptible to limited proteolysis in the apo form, but it becomes partly protected in the bound form. It was not possible to crystallize full-length Osh4 in the absence of any ligand, and this was attributed to disorder in the lid region in the apo state. The crystal structure of the apo form was, however, determined using a truncated form of Osh4 lacking the lid residues 1-29. The apo form features an unobstructed tunnel opening, and confirms that most of the remainder of the core protein structure does not change conformation when the lid is removed. However, helix α7 pivots around its N terminus such that the C terminus moves about 15 Å. In the bound form, the ε-amino groups of Lys109 and Lys336 are only ~3.6 Å away from each other and lie in an unusual and energetically unfavorable semi-buried environment (Fig. 1(b)). In the apo structure, these two residues move farther away from each other, and interact with bound sulfate ions of the crystallization medium. The bound sulfate ions coincide with a nearly planar surface surrounding the tunnel opening, and suggest potential phospholipid binding sites.

The multiple structural differences observed between the bound and apo conformations led to a model for sterol uptake and release.[11] In this model, interactions with the phospholipid membrane promote the opening of the lid. Osh4 then touches down on the membrane surface such that the tunnel opening is in direct contact with the membrane, allowing the sterol molecule to enter or exit without contacting bulk aqueous solvent. The conformational changes of Lys109 and Lys336, and helix α7 were proposed as potential components of the activation pathway for membrane-triggered lid opening. However, only two conformational states have been accessed by crystallography, so it has not been possible to derive a full picture of the conformational pathway of sterol exchange. To fill in this gap in our understanding of the mechanism of cholesterol uptake and release by Osh4, equilibrium molecular dynamics (MD) simulations of the Osh4 in apo and bound states, and a steered MD simulation of cholesterol egress from the bound state, were performed. The major findings are that the observed dynamics are consistent with a lid-opening model, and that the conformation of helix α7 is coupled to lid opening. The simulations provide for the first time the details of a step-wise mechanism for cholesterol egress from the Osh4 tunnel.

Results

Equilibrium MD of the Osh4-cholesterol complex

Throughout the 30 ns equilibrium simulation of the Osh4 cholesterol complex (Osh4-cho NPT, Table 1), cholesterol remains tightly bound in the tunnel. The 3-hydroxyl group of cholesterol maintains stable water-mediated hydrogen bonds to a cluster of polar side chains at the bottom of the tunnel. Cholesterol never forms any direct hydrogen bond with the protein during the simulation, consistent with the crystal structure. The first major structural transition of the simulation begins with a large movement of helix α7 at 5 ns (marked by the arrow in Fig. 2(a)). This transition results in a 9 Å movement of the α7 C terminus towards the lid (Fig. 2(b)). Throughout the rest of the simulation helix α7 undergoes wide swinging motion towards and away from the lid to a combined maximum displacement of 14 Å.

Individual Cα root-mean-square deviation (RMSD) analysis reveals several mobile regions (Fig. 2(c)). Lid residues 2-8 are highly mobile throughout the entire simulation. The hydrophobic residues Trp10, Phe13, Leu14, Ile17, and Phe20 that line the inner surface of the helix α1 of the lid remain tightly bound to the hydrophobic tail of cholesterol, as seen in the starting structure (Fig. 1(c)). In other words, spontaneous opening of the lid is not observed in the bound state. Residues 20-29 located on a loop of the lid have RMSD values in the range of 3-6 Å. These residues connect the α1 helix of the lid to the protein core. Dislocation of this loop leads to a slight opening in the tunnel entrance. The Lys109 - Lys336 distance increased from ~3.6 Å to a range of 6-9 Å

Table 1. List of the simulations performed, simulation time, and their conditions (k in units of kcal mol^{-1} Å^{-2})

Label	Time (ns)	Description
Osh4-cho NPT	30	Unrestrained NPT of Osh4–cholesterol complex
Osh4 NPT	50	Unrestrained NPT of Osh4
Osh4 Δ29 NPT	30	Unrestrained NPT of ligand-free truncated Osh4
Osh4-cho SMD	2, 10, and 20	First pulling direction using Cα of Leu161 as fixed atom; independent runs using a spring constant of k=0.5
Osh4-cho SMD2[a]	2, 10, and 20	First pulling direction using Cα of Leu161 as fixed atom; k=1.0
Osh4-cho SMD3[a]	2, 10, and 20	First pulling direction using Cα of Leu161 as fixed atom; k=5.0
Osh4-cho SMD4[a]	2, and 10	Second pulling direction by using Cα of Ile189 as fixed; k=0.5
Osh4-cho SMD5[a]	2, and 10	Third pulling direction by using Cα of Leu187 to Ile189 as fixed atoms; k=0.5

[a] Alternative SMD runs to explore the effects of varying pulling direction and force constant; excluded from detailed analysis.

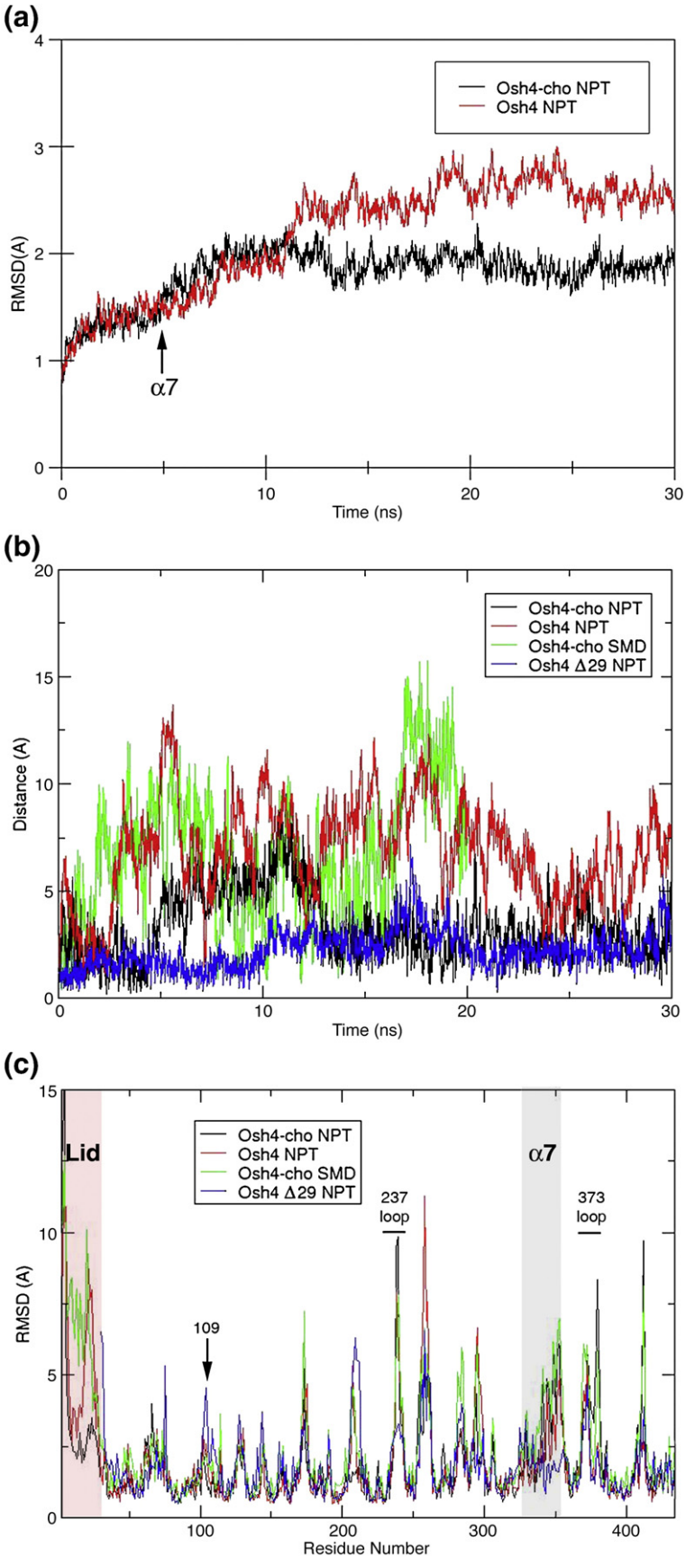

Fig. 2. (a) RMSD plot for the equilibrium simulation of Osh4-cholesterol complex (black, Osh4-cho NPT) and the ligand-free Osh4 (red, Osh4 NPT) as a function of simulation time. (b), Conformational flexibility of helix α7 measured by the displacement of its N terminus from the starting position as a function of simulation time. Equilibrium MD of Osh4-cholesterol (black, Osh4-cho NPT), steered MD of Osh4-cholesterol (green, Osh4-cho SMD), equilibrium MD of the ligand-free Osh4 (red, Osh4 NPT), and equilibrium MD of the Δ1-29 apo Osh4 construct (blue, Osh4 Δ29 NPT). (c) The Cα RMSD for equilibrium MD of Osh4-cholesterol (Osh4-cho NPT), steered MD of Osh4-cholesterol (Osh4-cho SMD), equilibrium MD of the ligand-free Osh4 (Osh4 NPT), and equilibrium MD of the Δ1-29 apo Osh4 construct (Osh4 Δ29 NPT) color-coded as in (b).

during the first 350 ps of the equilibrium simulation, thereby reducing the unfavorable electrostatic interaction between these two residues. During the rest of the simulation, the Lys pair did not return to the short distance seen in the starting structure. This is consistent with the notion that the short-range interaction between these two residues in the bound structure is highly unfavorable. The distances between the backbone atoms of these residues stay in the range of 14-16 Å during the entire simulation, as compared to 13.8 Å in the crystal structure. The lid does not open during the equilibrium simulation of the complex. This finding does not appear to be consistent with a coupling between opening and the inter-Lys separation, at least on the 30-50 ns time-scale of the simulations.

The mobility of the 237-239 loop seen in the simulation is consistent with experimental evidence for its flexibility.[11] Residues Gly237, Tyr238, and Phe239 located on a loop between β13 and β14 and Glu372 and Glu373 located on a loop connecting β18 and helix α8 have RMSD values of more than 6 Å and 4 Å, respectively. Both of these regions had high *B*-factors in the range 30-40 $Å^2$ in the crystal structure compared to an average *B*-factor of 25 $Å^2$ for the protein. Replacement of residues 237-239 was necessary for the crystallization of the ligand-free truncated form of Osh4. Thus the mobility of the 237-239 loop seen in the simulation is consistent with experimental evidence for its flexibility (Figs. 1 and 2(c)). These observations lend confidence that the varying degrees of mobility seen in the simulations in various parts of the structure provide a realistic reflection of the true dynamics of Osh4.

Equilibrium MD of ligand-free Osh4

To evaluate the stability of the structure of Osh4 in the ligand-free conformation, equilibrium MD simulations were performed after removing the cholesterol from the crystal structure of the complex (Osh4-NPT, Table 1). Initially a 30 ns unrestrained equilibrium simulation was carried out. With the important exception of the lid region, the structural changes seen in the apo simulation closely mirror those seen in the complex Fig. 2(c). These include similar changes in the Lys109, Lys336, and α7 regions. In a sharp contrast to the stable behavior of the lid in the bound state simulation, in the apo simulation the lid starts to move to a different conformation at ~10 ns. Residues 2-28 have the highest backbone RMSD values. Helix α1 of the lid (residues 8-18) has an RMSD of 3-6 Å while the loops of the lid (residues 2-7 and 19-25) have an RMSD between 6-9 Å. Between time zero and 20 ns, the N-terminal residues of the lid make and break transient interactions with α7. As the lid opens it interacts with helix α7 directly through a stacking interaction between the side chains of Tyr5 of the lid and Phe329 of helix α7 Fig. 3(c) and (d). In contrast, the stacking interactions between Tyr5 and Phe32, and Trp10 and Phe32 are broken. Residues 3-7 of the loop undergo a loop-to-helix transition around 20 ns, and after this point the transient interactions with α7 are no longer observed. The backbone RMSD is ~2 Å for most of the residues, except for those on the lid and loops (Fig. 2(b)). The structural change is linked to side chain rearrangements at the interface of the lid and the tunnel entrance (Fig. 3 (b)). However, the lid is not completely displaced from the tunnel entrance. The conformational change does not fully expose the hydrophobic residues on the inner surface of the lid and the entrance of the tunnel.

A principal component analysis[18,19] identified the lid opening transition as the dominant large-scale motion in the apo simulation (Osh4-NPT). We find that the motion described by the first principal axis in configuration space (i.e., the eigenvector corresponding to the largest eigenvalue; see Materials and Methods) is concentrated almost entirely in the lid region. Figure 4 shows the 30 ns trajectory projected onto this first principal axis. The sigmoidal trajectory is consistent with the above analysis: before ~10 ns, the lid is stably closed; at ~10 ns, the lid partly opens, and remains in that state for the remainder of the simulation. Consistent with this, the first principal axis evaluated using only the first half of the trajectory (which includes the lid opening event) is nearly identical with the first axis of the entire trajectory (angle cosine of ~0.89); whereas the first principal axis evaluated for the second half of the trajectory coincides with the second principal axis of the entire trajectory (angle cosine of ~0.85). As indicated by the inset in Fig. 4, the motions captured by the first principal axis consist of (1) an outward motion of the loop 19-25 and helix α1 away from the cholesterol site, and (2) a slight inward motion of helix α7 into the space vacated by the lid, which occur consecutively in the simulations.

Towards the end of the 30 ns run, we observed an increased opening of the tunnel entrance. We extended the simulation to 50 ns to see whether the lid becomes completely dislodged from the entrance of the tunnel in the absence of bound cholesterol. Between 30 ns and 50 ns, we observe further displacement of the lid from the rest of the protein that leads to additional openings between the lid and the tunnel rim (Supplementary Data Fig. S1). However helix α1 of the lid remains tethered to the tunnel through hydrophobic interactions of Trp10, Leu14, and Ile17 of the lid to Ile206, Leu207, and Val208 on the rim of the tunnel (Fig. 3(b)). Nevertheless, transient flipping out of the side chains of Phe20 and Leu27 into the solvent and the loop-to-helix transition of residues 2-7 contributed to an opening between the lid and the tunnel (Fig. 3(a) and S1b) at 30 ns. In summary, the equilibrium simulation of intact Osh4 in the absence of cholesterol indicates that the lid changes conformation with respect to the bound structure. However, the lid does not spontaneously open the tunnel enough to allow cholesterol exchange on the time-scale accessible to the simulations.

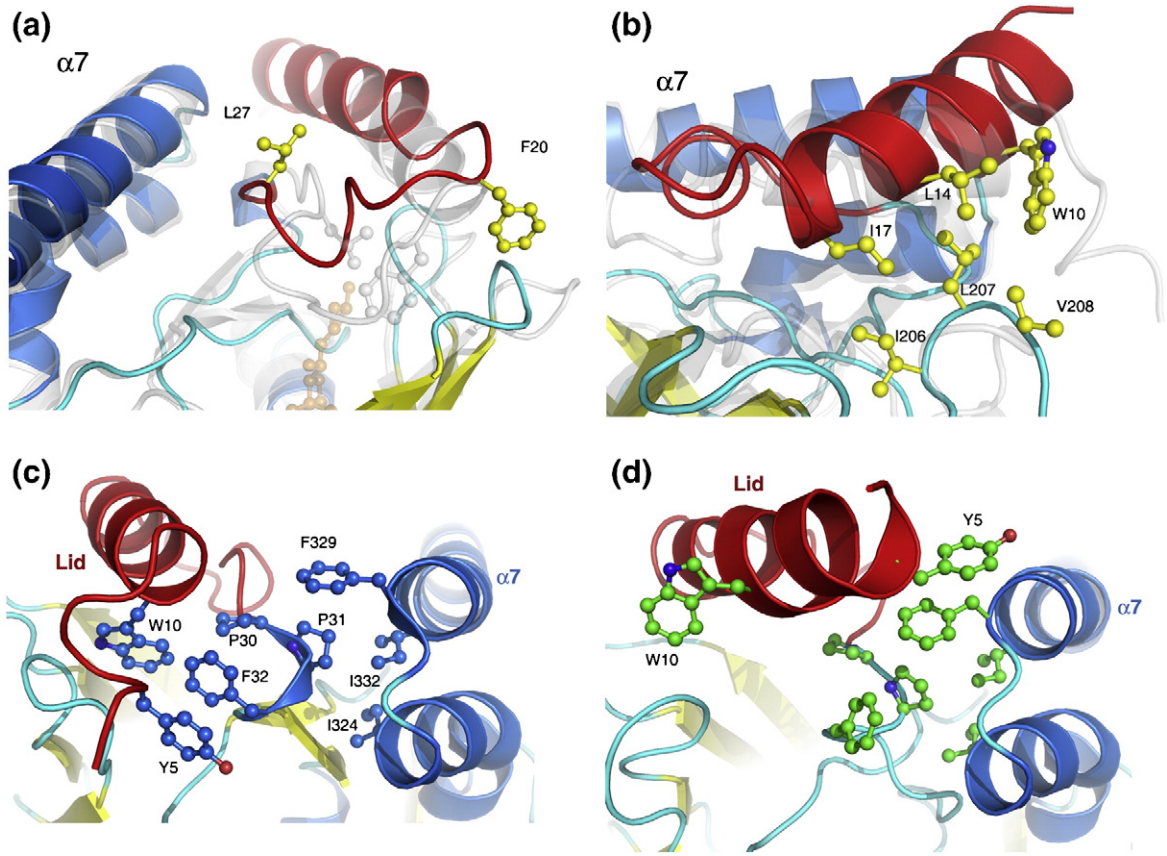

Fig. 3. Interactions between the lid and helix α7. (a) Equilibrium MD of full-length ligand-free Osh4 (Osh4 NPT). The lid (red) changes conformation relative to the starting structure (translucent) in the equilibrium simulation of apo Osh4. Phe20 and Leu27 are shown in a flipped-out conformation at 30 ns. (b) The lid remains anchored to the protein core through interactions between Trp10, Leu13, and Ile17 of the lid and Ile206, Leu207 and Val208 of the tunnel entrance (Osh4 NPT). (c) The Osh4-cholesterol complex (Osh4-cho NPT) compared to (d) the ligand-free Osh4 (Osh4NPT). The stacking interactions of Tyr5 and Trp10 with Phe32 observed in the Osh4-cholesterol complex have been replaced by a new stacking interaction between Tyr5 and Phe329 in the equilibrium simulation of ligand-free Osh4.

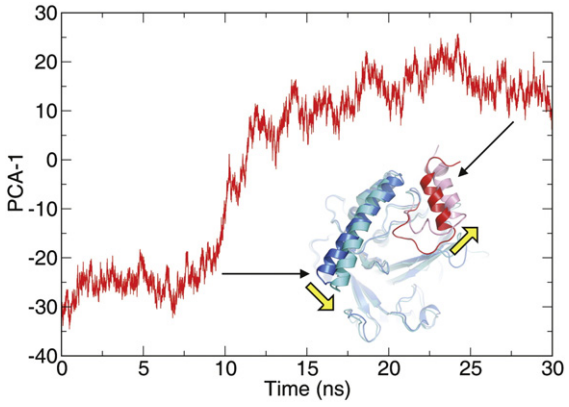

Fig. 4. Principal component analysis of ligand-free Osh4 (Osh4 NPT). A projection of the simulation trajectory onto the eigenvector corresponding to the largest eigenvalue is shown as a function of time. The inset shows an overlay of the starting (red lid and blue helix α7) and ending structures, with the direction of change indicated with the yellow arrows.

Equilibrium MD of ligand-free truncated Osh4

To further understand the influence of the lid on the mobility of helix α7 and the rest of the protein, a 30 ns equilibrium MD of the ligand-free truncated Osh4 was carried out (Osh4 Δ29 NPT, Table 1), starting from the energy-minimized crystal structure of the Δ1-29 truncated apo Osh4. Throughout the 30 ns simulation, helix α7 remains in essentially the same conformation as seen in the apo crystal structure (Fig. 2(b)). The backbone RMSD values of helix α7 remain in the range of 2-3 Å during most of the simulation (Fig. 2(c)). At around 17 ns helix α7 moves by a maximum displacement of ~7 Å. This is significantly less than the maximum displacement of ~15 Å seen during the equilibrium simulation of the ligand bound and the unbound full-length protein (Fig. 2(b)). The behavior of helix α7 in the truncated Osh4 simulation thus differs dramatically from the observations in the simulations of full-length Osh4. We expect this truncated Osh4 simulation to reflect the conformation of the fully open state. The results suggest that the conformation of helix α7 in the fully open state, unlike the conformation in the bound state, is stable.

Steered MD simulation of cholesterol release

The main goal of this study was to determine the microscopic steps involved in cholesterol exchange. Because this process does not occur spontaneously on the time-scale of tens of nanoseconds accessible to the simulations, we carried out steered MD to follow the trajectory of exchange. In those simulations, cholesterol is mechanically pulled out of the binding pocket by coupling it to a spring that moves away from the binding site at a constant pulling speed.

Simulations with different pulling speeds and spring constants produce consistent results (Osh4-cho SMD, SMD2-5, Table 1). Structurally, the steered MD simulations consistently show complete displacement of the lid of Osh4 and significant motion of helix α7, independent of spring constant and pulling speed. Energetically, the work *versus* extension curves from simulations with low pulling speeds (0.002 and 0.004 Å ps^{-1}) and soft spring constant (k=0.5 and 1 kcal mol^{-1} $Å^{-2}$; Osh4-cho SMD and SMD2, 4, and 5 in Table 1) agree nearly quantitatively up to extensions of ~15 Å, with a standard deviation of ~1.65 kcal $mol^{-1}$of the work curves from the mean. However, for faster pulling speeds (0.2 Å ps^{-1}) or stiffer pulling springs (k=5 1 kcal mol^{-1} $Å^{-2}$, Osh4-cho SMD3 in Table 1), substantially more work is performed, indicative of significant non-equilibrium dissipative effects in those runs. Correspondingly, the analysis described below focuses on a run at slow speeds and with soft springs (Osh4-cho SMD in Table 1).

During the steered MD simulations, cholesterol encounters three main energy barriers as it moves along the tunnel opening: one at a distance of around 1 Å from the starting position, the second at 7 Å, and the last one after around 13 Å (Fig. 5(a)). Before crossing each barrier, cholesterol effectively stalls and the applied force grows linearly with time. Eventually, the force is sufficiently large to break the interactions responsible for the resistance.

Integration of the force extension curve gives the work performed on the cholesterol as it is pulled out of the binding pocket. The amount of work W done

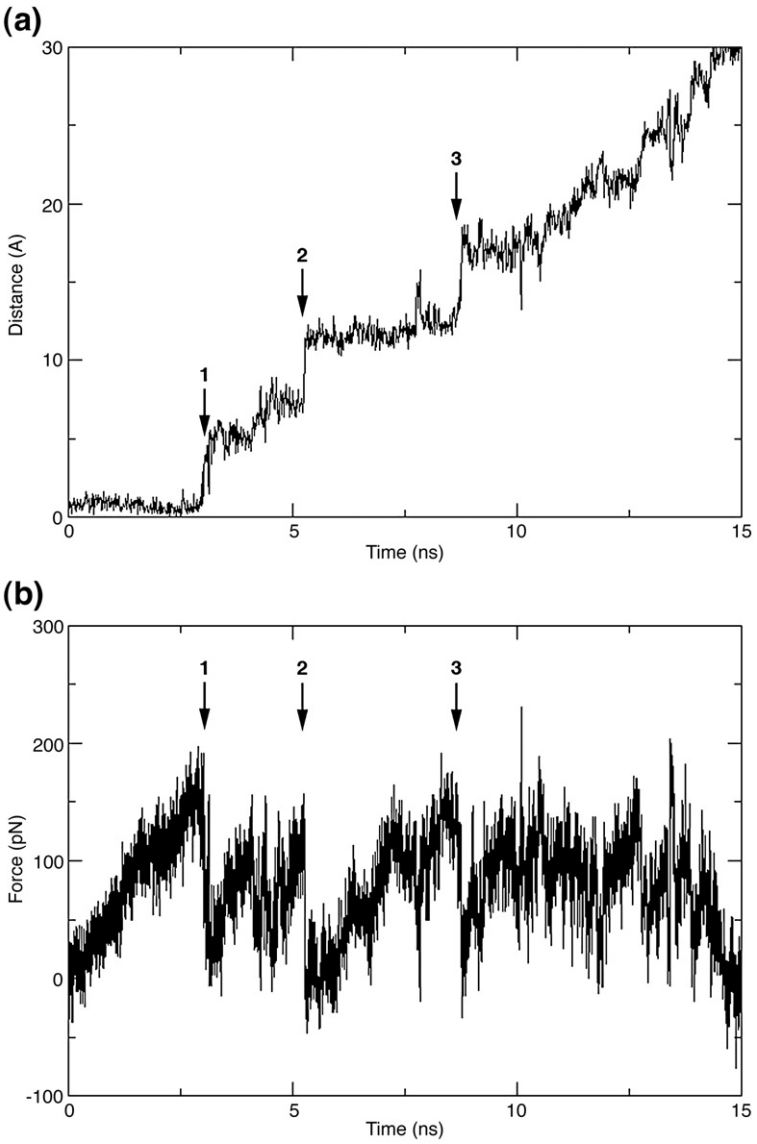

Fig. 5. Steered MD of cholesterol egress from Osh4 (Osh4-cho SMD). (a) Extension *versus* time plot of Osh4-cholesterol from steered MD at a pulling speed of 0.002 Å ps^{-1}. (b) Force-extension profile of Osh4-cholesterol steered MD at a pulling speed of 0.002 Å ps^{-1}.

to overcome the first barrier where the hydrogen bonds mediated through water molecules are broken is about 8 kcal mol^{-1}. Similarly, the second barrier where interaction between the lid and the entrance of the tunnel is broken requires another ~6 kcal mol^{-1} of work. The actual free energy barriers are expected to be lower according to the second law of thermodynamics, $\Delta G \leq \langle W \rangle$. Once the non-covalent bonds are broken at each energy barrier, large displacements or slips of cholesterol are observed as it moves along the tunnel.

At the beginning of the simulation, cholesterol makes several hydrogen bonds through water molecules. A cluster of ordered water molecules hydrating the side chains of Trp46, Tyr97, Asn165, and Gln181 at the bottom of the pocket coordinate the interaction between the cholesterol 3-hydroxyl group and the protein (Figs. 1(c) and 6(a)). During the initial phase of the simulation few transient hydrogen bonds are observed between cholesterol and protein through the side chains of Gln96, Asn165, Gln181 and the main chain of Phe42, and Ile167. As the force applied on cholesterol increases, these hydrogen bonds are broken, enabling cholesterol to move up the tunnel (Fig. 6(b)).

As cholesterol is pulled away from the starting position, its hydrophobic tail adopts a bent conformation that is pressed against the lid. Cholesterol encounters the second barrier after being pulled 7 Å from its starting position. The hydrophobic tail of cholesterol opens the lid as it overcomes the second barrier (Figs. 5(a) and 6(c)). Strong interactions between the hydrophobic residues that line the lid and the rim of the tunnel are broken. The largest conformational change induced by the forced extraction of cholesterol occurs at this transition, following the complete dislocation of the lid from the mouth of the tunnel (Figs. 2(c) and 6(d)). The backbone RMSD of residues 2-20 of the lid increases to more than 6 Å. Trp10 moves by as much as 10 Å from its original position. Helix α7 also undergoes large conformational fluctuations similar to those seen during the equilibrium MD of the complex and the ligand-free Osh4 (Fig. 2(b)). The rest of the protein remains stable

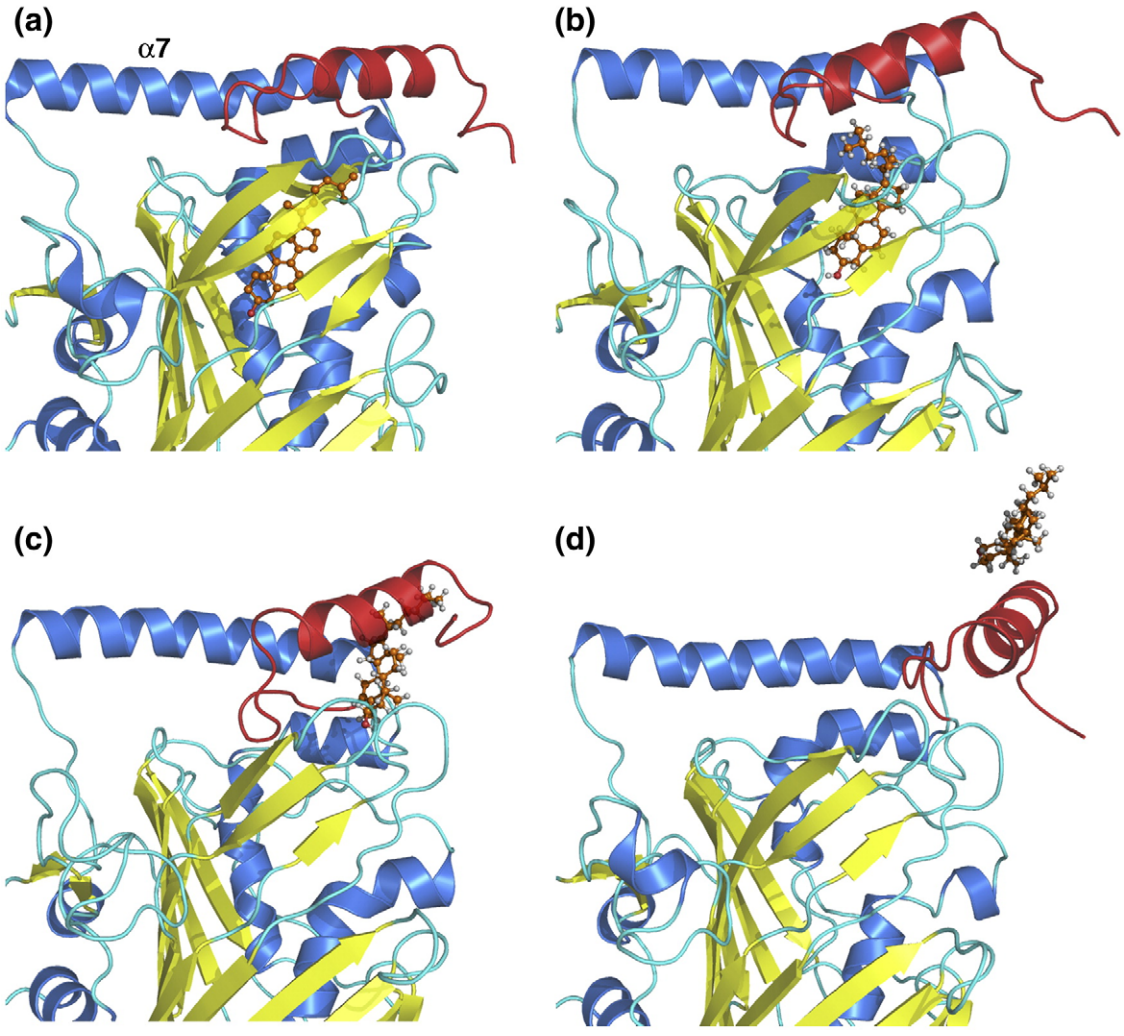

Fig. 6. Stepwise pathway for cholesterol egress in the Osh4-cho SMD simulation. Representative configurations of the complex from the simulated ensemble: (a) time zero; (b) 3.2 ns; (c) 5.6 ns; and (d), 15.5 ns. The total simulation time was 20 ns.

with RMSD values of 1-2 Å as seen from the analysis of backbone RMSD (Fig. 2(c)).

As the cholesterol is pulled further from its starting position, it makes a few transient interactions with side chains of Ser6 of the lid, and Ser106 and the main chains of Leu24, and Glu107 at the entrance of the tunnel (Fig. 6(d)). Cholesterol forms new hydrophobic interactions with the hydrophobic residues on the lid while breaking other interactions. The third and final barrier is overcome when these interactions are broken.

Discussion

The MD simulations provide a consistent and energetically reasonable pathway for cholesterol exchange by Osh4. Equilibrium and steered MD simulations carried out with different force constants and steering velocities (Osh4-cho SMD, SMD2-5) lead to qualitatively similar pictures. Cholesterol dissociates from Osh4 in a stepwise fashion. The upper bounds to the free energy barriers encountered for the main steps, 6 and 8 kcal mol^{-1} in the Osh4-cho SMD simulation selected for analysis are not prohibitive. Indeed, cholesterol transfer rates of $\sim$0.15 s^{-1} were recently obtained experimentally, roughly consistent with a combined barrier of $\sim$14 kcal mol^{-1} for a pre-factor of about 1 ns^{-1}.[12]

During the forced cholesterol unbinding, there is little change to the overall structure of Osh4, excluding those regions shown experimentally to be conformationally labile. First, water-mediated hydrogen bonds at the bottom of the pocket are disrupted. Second, the lid opens to allow access to solvent. Third, cholesterol slides out of the tunnel, making and breaking transient contacts with the tunnel wall, tunnel rim, and the hydrophobic face of the lid.

Helix α7 is the region that moves the most between the bound and apo crystal structures of Osh4.[11] One of the objectives of this study was to investigate whether the movement of α7 is coupled to lid opening. The lid and helix α7 lie next to each other, suggesting that α7 might in some way regulate, or be regulated by, the conformation of the lid. The conformation of α7 observed in the apo structure appeared to be more compatible with membrane binding, because it fits the profile of a flat membrane-docking surface surrounding the tunnel opening. Helix α7 is highly mobile in the equilibrium MD simulations of both the complex (Osh4-cho NPT) and the ligand-free form (Osh4 NPT). The C terminus of the helix pivots around its N terminus towards and away from the lid throughout the simulation, moving by about 15 Å overall. It is the only major region of secondary structure in the complex that is not stable in the starting conformation derived from the crystal structure. The observations show that the bound-state conformation of α7 observed in the crystal is marginally stable, and probably reflects its participation in lattice contacts in the crystal of the bound form.

To probe whether the movement of helix α7 was coupled to a shift in the lid, principal component analysis was applied to the equilibrium MD simulation of the ligand-free Osh4 (Osh4 NPT). This analysis showed a coupling between the shift in the lid away from the tunnel entrance with a shift in helix α7 closer to the entrance. The overall direction of the shift corresponds approximately to the shift between the crystal structures of the bound and apo states. In the steered MD, similarly high mobility of α7 is seen throughout the simulation. The nature of the dynamics does not appear to be closely coupled to the progress along the coordinate of cholesterol egress or the conformation of the lid. At no point in any of these simulations does α7 move all the way to the conformation observed in the crystallized apo state, in which the lid is absent from the protein construct. α7 was relatively stable in the equilibrium simulation of the apo structure of the lid-deleted Osh4 mutant (Osh4 Δ29 NPT), starting from the crystal structure of this form. Taken together, these observations suggest that the closed conformation of the lid promotes a meta-stable, high-mobility conformation of α7, while the open conformation of the lid is compatible with a stable, lower-mobility conformation. The stability of helix α7 in the apo state (Osh4 Δ29 NPT), and the coupling of its conformation to lid opening are likely to have an important regulatory significance, since the open-state conformation of α7 appears to be the most compatible with membrane docking, as discussed below. This point would be potentially interesting to explore using engineered disulfide crosslinks to limit the mobility of α7.

One of the more surprising observations from the crystal structures of Osh4 complex was that the ε-amino groups of Lys109 and Lys336 are located only $\sim$3.6 Å away from each other.[11] These residues are of special interest because they are critical for Osh4 function, but they are not involved directly in cholesterol binding. The short-range interaction was not observed in the apo structure, in which these side-chains are farther from each other, and form new interactions with sulfate ions of crystallization that were not present in the bound-state structure. These sulfate ions are coplanar with the tunnel entrance. The geometry of the interactions suggests that the sulfate ions mimic a physiological interaction with the phosphate groups of membrane phospholipids. It was therefore proposed that upon interaction with the membrane this unfavorable interaction would drive apart the Lys residues and promote the open conformation necessary for cholesterol exchange. In our simulations, the ε-groups of these lysine residues move to about 9 Å from each other within the first 50 ps in both equilibrium and steered simulations (Osh4-cho NPT, Osh4 NPT, Osh4-cho SMD). However the main chains of these residues take much longer to move away from each other towards the distance observed in the open conformation. The MD simulation data support the concept that the close juxtaposition of the Lys residues observed in the bound-state crystal structure is unstable. How-

ever, the Lys residues have ample freedom to move apart very early in the simulation, and it does not appear that this movement alone is a driving force for lid opening. As a possible functional role, these residues could facilitate the docking of the tunnel rim area to acidic phospholipid membranes for cholesterol exchange.

Cholesterol transfer dynamics have been examined by similar steered MD simulations for the START domains of steroidogenic acute regulatory protein (StAR) and metastatic lymph node 64 (MLN64). Like Osh4, cholesterol-binding START domains bind cholesterol in a tunnel that is completely inaccessible to solvent.[20,21] One objective of the START domain dynamics study was to determine whether a wholesale conformational change into a molten globule[22] was necessary for cholesterol exchange, or whether the opening of a small region over the binding site was sufficient. The simulations showed that only local changes in the conformation of the protein occurred during the release of cholesterol.[23] Steering cholesterol out of the cavity resulted mainly in the transient opening of omega loop 1. The backbone RMSD of loop residues increased to as much as 14 Å during the simulation. The remaining residues were stable with an RMSD range of 2-3 Å. Our results for the representative ORP Osh4 are thus similar to the previous results for START domains, suggesting that tunnel opening via localized lid displacement is a widespread mechanism for cholesterol exchange by soluble proteins.

In its physiological reaction, Osh4 exchanges cholesterol with membranes. The main limitation of this study is that the membrane was omitted. Nevertheless, some inferences about the transfer reaction can be drawn. From the crystal structures, it is clear that the uptake from, and release to membranes of cholesterol by Osh4 requires the opening of the cholesterol-binding tunnel. The simulations described here show how this opening could occur in practice. The last and greatest energy barrier to cholesterol release to solution in the simulation occurs when van der Waals contacts between cholesterol and hydrophobic residues of the Osh4 lid and tunnel rim are broken. These hydrophobic moieties are then exposed to aqueous solution. In the membrane context, these moieties would be exposed instead to interactions with membrane lipids. Thus, in the membrane context, where these residues would have access to the hydrocarbons of the phospholipid tails, we expect that this final energy barrier would be greatly diminished. Rather, the largest energy barrier, and therefore the rate-limiting step, would be the opening of the lid.

In the extended equilibrium simulation of the apo conformation of full-length Osh4 (Osh4 NPT), the lid changed conformation with respect to the starting structure, but did not open spontaneously. The spontaneous opening of the lid in aqueous solution is energetically unfavorable and therefore a rare event, consistent with the simulation results. In a recent study an ALPS (ArpGAP1 lipid packing sensor) motif was identified within the lid of Osh4.[24] The ALPS motif in Osh4 and in other proteins interacts preferentially with curved membranes. In our working model of the membrane exchange reaction, binding of the ALPS motif to the membrane would force the lid into the open conformation. This in turn would trigger helix α7 to move into the apo conformation, favoring stable membrane docking. It will be interesting to explore this question further with simulations of Osh4 in the presence of a phospholipid membrane.

Materials and Methods

System setup

The 1.6 Å resolution crystal structure of Osh4 in complex with cholesterol (PDB entry code 1ZHY) was used as the starting model. Crystallographic water molecules were retained. The hydrogen atoms of all protein residues and water molecules were generated with the PSFGEN plug-in of the Visual Molecular Dynamics (VMD) program.[30] The system was solvated in a cell of size 75 Å×72 Å×96 Å filled with 13,370 TIP3P water molecules. Eleven sodium and two chloride ions were added to neutralize the system for all simulations except Osh4-Δ29 NPT. For Osh4-Δ29 NPT, 16 sodium and one chloride ion were added. The dimensions of the water cell were chosen to accommodate the displacement of cholesterol by 40 Å from its bound position. The final system contained a total of 47,130 atoms.

MD simulations

All simulations were performed using the program NAMD[25] and CHARMM27 force-fields.[26] Periodic boundary conditions were imposed. The system was first minimized for two consecutive 2000 conjugated gradient steps, where the protein was held fixed and water molecules were allowed to move; subsequently, all atoms except the protein backbone were allowed to move. After minimization, the system was equilibrated for 200 ps with restraints using a force constant of 0.5 kcal mol^{-1} $Å^{-2}$. An integration step of 1 fs and uniform dielectric constant of 1 were used throughout the simulation. A multiple time-step integration algorithm was employed to evaluate covalent bond interaction every time-step, short-range non-bonded interactions every two time-steps, and long-range electrostatics every four time-steps. Full electrostatics were computed using the particle-mesh Ewald method with a grid size of 75 Å×75 Å×96 Å. A 12 Å cutoff was applied. All MD runs were carried out at constant temperature and pressure (NPT). The pressure was maintained at 1 atm (101,325 Pa) using the Langevin piston method, and the temperature was controlled by using Langevin dynamics at 300 K with a damping coefficient of 5 ps^{-1}. A Langevin piston period of 100 fs and a damping time constant of 50 fs were employed for pressure control. After minimization and restrained equilibration, production runs were carried out at NPT.

We used principal component analysis to filter out large-scale motions in the equilibrium MD simulations.[18,19] The N Cα backbone atoms along the trajectories were aligned and a 3 N×3 N covariance matrix was calculated that describes the correlated fluctuations in Cartesian coordinate space. The simulation trajectory was then projected onto the eigenvectors of this covariance matrix. Eigenvectors for

large eigenvalues correspond to motions with the largest amplitude in a Cartesian-space representation.

Constant velocity steered MD of cholesterol were performed using different spring constants and velocities (Table 1). Three pulling velocities of 0.02 Å ps^{-1}, 0.004 Å ps, and 0.002 Å/ps were chosen. Spring constants k of 5 kcal/mol/Å^2, 1 kcal/mol/Å^2, and 0.5 kcal/mol/Å^2 were used. The pulling force was applied along the vector pointing from fixed Cα atoms at the end of the tunnel to the center of mass of cholesterol. Cα atoms of Leu161, Ile189, or Leu187 to Ile189 were used as fixed positions for independent runs. The work along each of the pulling directories is defined as a contour integral along the force-extension curve,

$$W(t) = \int_{z(0)}^{z(t)} F dz, \quad (1)$$

where $F=F(t)$ is the force and $z=z(t)$ is the distance between the two force centers. Up to an arbitrary constant, the free energy (or potential of mean force) $\Delta G(z)$ along z can then be obtained from repeated steered molecular dynamics simulations:[27,28]

$$e^{-\Delta G(z)/k_B T} = \langle \delta[z - z(t)] e^{[W(t)-V(0)]/k_B T} \rangle. \quad (2)$$

Equation (2) is an extension of Jarzynki's identity,[29] where k_B is Boltzmann's constant, and T is the absolute temperature. Here, the potential energy $V(0)$ stored in the pulling spring at the beginning of the simulations is approximately zero and will be neglected. Moreover, because the number of simulations is small and hysteresis effects are significant, we cannot estimate $\Delta G(z)$ with confidence; instead, we invoke the second law of thermodynamics to obtain an upper bound, $\Delta G(z) \leq \langle W\text{-}V(0) \rangle_z$, where the average is taken over the work when the trajectories cross z.

VMD[30] was used for trajectory processing and analysis of RMSD values, interatomic distance, and force. Figures were generated with PyMol†.

Acknowledgements

We thank Zoe Cournia and Jeremy Smith for sending us their parameter set for cholesterol. This work was supported by the intramural program of the NIDDK, National Institutes of Health.

Supplementary Data

Supplementary data associated with this article can be found, in the online version, at doi:10.1016/j.jmb.2008.01.075

References

1. Yeagle, P. L. (1985). Cholesterol and the cell membrane. *Biochim. Biophys. Acta*, **822**, 267–287.
2. Simons, K. & Ikonen, E. (2000). Cell biology - how cells handle cholesterol. *Science*, **290**, 1721–1726.
3. Goldstein, J. L., DeBose-Boyd, R. A. & Brown, M. S. (2006). Protein sensors for membrane sterols. *Cell*, **124**, 35–46.
4. Liscum, L. & Munn, N. J. (1999). Intracellular cholesterol transport. *Biochim. Biophys. Acta*, **1438**, 19–37.
5. Maxfield, F. R. & Menon, A. K. (2006). Intracellular sterol transport and distribution. *Curr. Opin. Cell Biol.* **18**, 379–385.
6. Levine, T. & Loewen, C. (2006). Inter-organelle membrane contact sites: through a glass, darkly. *Curr. Opin Cell Biol.* **18**, 371–378.
7. Olkkonen, V. M., Johansson, M., Suchanek, M., Yan, D., Hynynen, R., Ehnholm, C. *et al.* (2006). The OSBP-related proteins (ORPs): global sterol sensors for co-ordination of cellular lipid metabolism, membrane trafficking and signalling processes? *Biochem. Soc. Trans.* **34**, 389–391.
8. Kandutsch, A. A. & Shown, E. P. (1981). Assay of oxysterol-binding protein in a mouse fibroblast, cell-free system. Dissociation constant and other properties of the system. *J. Biol. Chem.* **256**, 13068–13073.
9. Olkkonen, V. M. & Levine, T. P. (2004). Oxysterol binding proteins: in more than one place at one time? *Biochem. Cell Biol.* **82**, 87–98.
10. Suchanek, M., Hynynen, R., Wohlfahrt, G., Lehto, M., Johansson, M., Saarinen, H. *et al.* (2007). The mammalian oxysterol-binding protein-related proteins (ORPs) bind 25-hydroxycholesterol in an evolutionarily conserved pocket. *Biochem. J.* **405**, 473–480.
11. Im, Y. J., Raychaudhuri, S., Prinz, W. A. & Hurley, J. H. (2005). Structural mechanism for sterol sensing and transport by OSBP-related proteins. *Nature*, **437**, 154–158.
12. Raychaudhuri, S., Im, Y. J., Hurley, J. H. & Prinz, W. A. (2006). Nonvesicular sterol movement from plasma membrane to ER requires oxysterol-binding protein-related proteins and phosphoinositides. *J. Cell Biol.* **173**, 107–119.
13. Sullivan, D. P., Ohvo-Rekila, H., Baumann, N. A., Beh, C. T. & Menon, A. K. (2006). Sterol trafficking between the endoplasmic reticulum and plasma membrane in yeast. *Biochem. Soc. Trans.* **34**, 356–358.
14. Beh, C. T. & Rine, J. (2004). A role for yeast oxysterol-binding protein homologs in endocytosis and in the maintenance of intracellular sterol-lipid distribution. *J. Cell Sci.* **117**, 2983–2996.
15. Beh, C. T., Cool, L., Phillips, J. & Rine, J. (2001). Overlapping functions of the yeast oxysterol-binding protein homologues. *Genetics*, **157**, 1117–1140.
16. Wang, P., Weng, J. & Anderson, R. G. W. (2005). OSBP is a cholesterol-regulated scaffolding protein in control of ERK1/2 activation. *Science*, **307**, 1472–1476.
17. Perry, R. J. & Ridgway, N. D. (2006). Oxysterol-binding protein and vesicle-associated membrane protein-associated protein are required for sterol-dependent activation of the ceramide transport protein. *Mol. Biol. Cell*, **17**, 2604–2616.
18. García, A. E., Blumenfeld, R., Hummer, G. & Krumhansl, J. A. (1997). Multi-basin dynamics of a protein in a crystal environment. *Physica D*, **107**, 225–239.
19. García, A. E. (1992). Large-amplitude nonlinear motions in proteins. *Phys. Rev. Lett.* **68**, 2696–2699.
20. Tsujishita, Y. & Hurley, J. H. (2000). Structure and lipid transport mechanism of a StAR-related domain. *Nature Struct. Biol.* **7**, 408–414.
21. Romanowski, M. J., Soccio, R. E., Breslow, J. L. & Burley, S. K. (2002). Crystal structure of the Mus

† http://www.pymol.org

musculus cholesterol-regulated START protein 4 (StarD4) containing a StAR-related lipid transfer domain. *Proc. Natl Acad. Sci. USA*, **99**, 6949–6954.
22. Christensen, K., Bose, H. S., Harris, F. M., Miller, W. L. & Bell, J. D. (2001). Binding of steroidogenic acute regulatory protein to synthetic membranes suggests an active molten globule. *J. Biol. Chem.* **276**, 17044–17051.
23. Murcia, M., Faraldo-Gomez, J. D., Maxfield, F. R. & Roux, B. (2006). Modeling the structure of the StART domains of MLN64 and StAR proteins in complex with cholesterol. *J. Lipid Res.* **47**, 2614–2630.
24. Drin, G., Casella, J. F., Gautier, R., Boehmer, T., Schwartz, T. U. & Antonny, B. (2007). A general amphipathic alpha-helical motif for sensing membrane curvature. *Nature Struct. Mol. Biol.* **14**, 138–146.
25. Phillips, J. C., Braun, R., Wang, W., Gumbart, J., Tajkhorshid, E., Villa, E. *et al.* (2005). Scalable molecular dynamics with NAMD. *J. Comput. Chem.* **26**, 1781–1802.
26. MacKerell, A. D., Feig, M. & Brooks, C. L. (2004). Improved treatment of the protein backbone in empirical force fields. *J. Am. Chem. Soc.* **126**, 698–699.
27. Hummer, G. & Szabo, A. (2005). Free energy surfaces from single-molecule force spectroscopy. *Accts Chem. Res.* **38**, 504–513.
28. Hummer, G. & Szabo, A. (2001). Free energy reconstruction from nonequilibrium single-molecule pulling experiments. *Proc. Natl Acad. Sci. USA*, **98**, 3658–3661.
29. Jarzynski, C. (1997). Nonequilibrium equality for free energy differences. *Phys. Rev. Lett.* **78**, 2690–2693.
30. Humphrey, W., Dalke, A. & Schulten, K. (1996). VMD: Visual molecular dynamics. *J. Mol. Graph.* **14**, 33–38.